Article

Non-Gaussian statistics of the order parameter across a phase transition

https://doi.org/10.1038/s41586-026-10811-1

Received: 21 July 2025

Accepted: 16 June 2026

Published online: 22 July 2026

Check for updates

Maxime Allemand[1,6], Géraud Dupuy[1,6], Paul Paquiez[1,6], Nicolas Dupuis[2], Adam Rançon[3,4], Tommaso Roscilde[5], Thomas Chalopin[1] & David Clément[1]✉

Second-order phase transitions are characterized by critical scaling and universality[1]. The singular behaviour of thermodynamic quantities at the transition, in particular, is determined by critical exponents of the universality class of the transition. However, critical properties are also characterized by the probability distribution of the order parameter across the transition[2,3], in which non-Gaussian statistics are expected[4–6], but remain largely unexplored[7]. Here, making use of single-atom-resolved detection in momentum space[8], we measure the full probability distribution of the order-parameter amplitude across a continuous phase transition in an interacting lattice Bose gas[9]. We find that fluctuations are captured by an effective potential—reconstructed from the measured probability distribution by analogy with Landau theory[10]—displaying a non-trivial minimum in the superfluid (ordered) phase, which vanishes at the transition point. Moreover, we observe non-Gaussian statistics of the order parameter near the transition, distinguished by non-zero high-order cumulants undergoing abrupt sign changes. We show numerically that these sign changes of the cumulants obey critical scaling in homogeneous systems, and that their experimental behaviour is not reproduced by classical models, whereas it is captured by a low-temperature quantum model. Our results underscore the crucial role of order parameter statistics in probing critical phenomena and universality.

Continuous phase transitions driven by spontaneous symmetry breaking[10,11] are fundamental phenomena covering all branches of physics[12]. The concept of a fluctuating order parameter ψ plays an essential part in their description. Its average amplitude $\langle|\psi|\rangle$ was shown by Landau[10] to distinguish the ordered phase, in which it assumes a non-zero value in the thermodynamic limit, from the disordered phase, in which it vanishes. Landau's mean-field theory, however, neglects fluctuations in the order parameter and fails to capture the singular behaviour at the transition, that is, the critical regime.

These phenomena are driven by the large fluctuations that develop as the system approaches the phase transition. As shown in Fig. 1a, this aspect is captured by the divergence of the correlation length ξ of the local order parameter, $\langle\psi^{\dagger}(0)\psi(x)\rangle_{c} \propto \exp(-|x|/\xi)$ (refs. 12,13). As this length grows beyond microscopic scales (for example, the interparticle distance), it reaches the Ginzburg length ℓ_{G}, marking the onset of the critical regime. The latter is characterized by power-law singularities of thermodynamic quantities, exhibiting universal critical exponents. These features are well understood in the framework of Wilson's renormalization group[14,15]. Systems that exhibit the same large-scale behaviour near their critical points are classified in the same universality class (that is, with the same critical exponents), despite having different microscopic physics. In finite-size systems, a peculiar behaviour appears within the critical regime when the correlation length ξ becomes larger than the linear system size L. Whereas for $\xi < L$, the central limit theorem (CLT) implies that the order-parameter statistics are Gaussian; when $\xi > L$, the CLT breaks down, and the order-parameter statistics become non-Gaussian[4–6].

The probability distribution function (PDF) of the order parameter, which fully captures its statistical properties, is a fundamental quantity in the description of phase transitions. At the transition point, its non-Gaussian shape is universal, that is, it depends on the universality class of the transition as well as global geometric properties (for example, boundary conditions, aspect ratio between different dimensions). The PDF has received extensive theoretical and numerical attention over the past few decades[2,16–20], focusing on the thermodynamic limit, where ξ and L are sent to infinity at fixed ξ/L. From an experimental perspective, however, measuring the non-Gaussian PDF at criticality poses a lot of challenges. The non-Gaussian regime is a narrow region of the control parameter near the transition point (Fig. 1a) that shrinks with increasing system size. In a macroscopic system with Avogadro number of particles, it reduces to the critical point, requiring, therefore, an unrealistic precision in the tuning of the control parameter. Furthermore, characterizing critical non-Gaussian statistics is inherently difficult[21], and, to our knowledge, has only been reported in a classical, mesoscopic system of liquid crystals[7,22]. More generally, non-Gaussian statistics are a diagnostic of complexity and criticality in physics and across many real-world phenomena[23], and their characterization is fundamental to the understanding of complex systems.

[1]Université Paris-Saclay, Institut d'Optique Graduate School, CNRS, Laboratoire Charles Fabry, Palaiseau, France. [2]Laboratoire de Physique Théorique de la Matière Condensée, Sorbonne Université, CNRS, Paris, France. [3]UMR 8523 (PhLAM – Laboratoire de Physique des Lasers Atomes et Molécules), University of Lille, CNRS, Lille, France. [4]Institut Universitaire de France, Paris, France. [5]Laboratoire de Physique, University of Lyon, Ens de Lyon, CNRS, Lyon, France. [6]These authors contributed equally: Maxime Allemand, Géraud Dupuy, Paul Paquiez. ✉e-mail: david.clement@institutoptique.fr

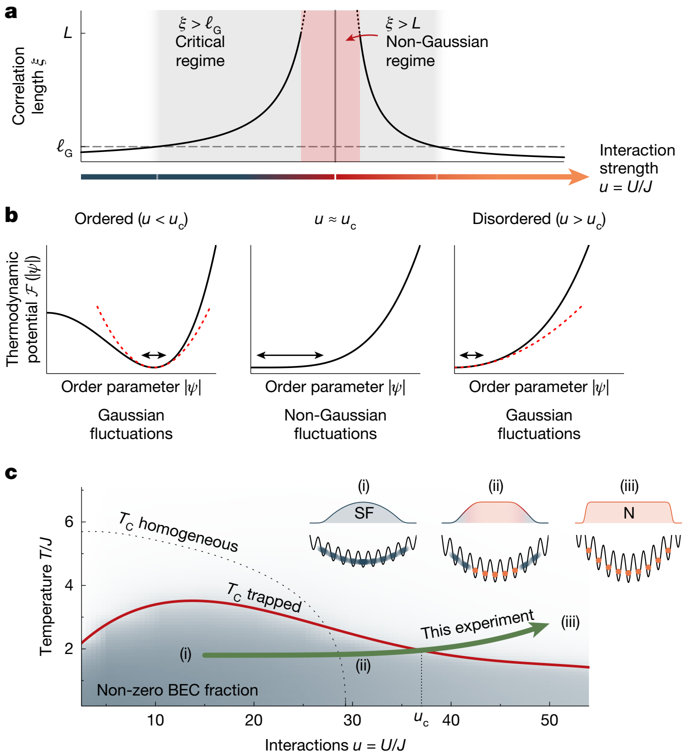

Fig. 1 | Continuous phase transitions. a, The critical regime (grey area) is reached when the correlation length ξ exceeds the Ginzburg length ℓ_G. Closer to the transition point, ξ exceeds the system size L, and non-Gaussian statistics are expected (red area). **b**, The critical properties of the transition are described by an effective thermodynamic potential $\mathcal{F}(|\psi|)$—analogous to the Landau free energy—which describes enhanced and non-Gaussian fluctuations of the order-parameter amplitude $|\psi|$ near the transition. **c**, We explore the superfluid-to-normal fluid phase transition of the Bose–Hubbard model, implemented by ultracold lattice bosons. A harmonic trap affects the interaction-dependent critical temperature $T_c(u)$ between a superfluid (blue region, i) and a normal gas (finite-temperature Mott insulator, white region, iii). Near the critical regime (ii), both phases coexist, with a normal core surrounded by superfluid shells.

Modern experimental platforms implement quantum many-body models in which phase transitions with substantial non-Gaussian critical regimes are expected, because of small system sizes of tens to hundreds of particles[24–31]. In these platforms, single-particle-resolved detection methods[32] provide access to the full counting statistics of observables[28,30,33–36]. These advances enable the exploration of the universal order-parameter statistics, which is complementary to the standard measurements of critical exponents[37–40].

Here, we leverage these techniques to measure the distribution of the condensate order parameter across the superfluid transition, using an ultracold gas of about 4,000 bosons in optical lattices (Fig. 1c). Our main results are threefold. First, we observe non-Gaussian order-parameter statistics in the critical regime near the transition, thereby providing a confirmation of renormalization group predictions[18]. Second, we show that the measured PDFs are well approximated by a phenomenological approach similar in spirit to Landau's[10]. Furthermore, we explain why this simple picture effectively describes our measurements. Third, we characterize the non-Gaussian nature of the statistics through high-order cumulants of the order-parameter amplitude $|\psi|$, and we reveal abrupt sign changes of these cumulants across the transition. We show numerically that these sign changes of cumulants exhibit critical scaling across the transition in homogeneous systems and that their experimentally observed behaviour is not captured by classical models, but is reproduced by a low-temperature quantum model with the same universal behaviour as that of lattice bosons. The characterization of the behaviour of the cumulants stems from the unique level of diagnostics offered by quantum simulators. It represents a new perspective on the fundamental nature of critical fluctuations[5,41,42].

Our experiment investigates the superfluid-to-normal fluid transition in a lattice Bose gas. We adiabatically load ultracold metastable helium (^{4}He*) atoms in a cubic optical lattice[43], realizing the Bose–Hubbard model (BHM):

$$\widehat{H} = -J\sum_{\langle \mathbf{i},\mathbf{j}\rangle}[\hat{a}_{\mathbf{i}}^{\dagger}\hat{a}_{\mathbf{j}} + \mathrm{h.c.}] + \frac{U}{2}\sum_{\mathbf{i}}\hat{n}_{\mathbf{i}}(\hat{n}_{\mathbf{i}}-1) + \sum_{\mathbf{i}} V_{\mathbf{i}}\hat{n}_{\mathbf{i}}. \tag{1}$$

Here, J and U designate the tunnelling and on-site interaction energies, respectively, $\hat{a}_{\mathbf{i}}^{\dagger}$ and $\hat{a}_{\mathbf{i}}$ are the bosonic creation and annihilation operators, respectively, on site $\mathbf{i}$, $\hat{n}_{\mathbf{i}} = \hat{a}_{\mathbf{i}}^{\dagger}\hat{a}_{\mathbf{i}}$ is the number operator and $\langle \mathbf{i},\mathbf{j}\rangle$ indicates nearest-neighbour lattice sites. The effect of the harmonic trapping potential is encoded in the spatial dependence of $V_{\mathbf{i}}$ (Methods). At zero temperature, the homogeneous BHM ($V_{\mathbf{i}} = 0$) features a quantum phase transition between a superfluid state and a Mott insulating state[44], occurring for a critical value u_c of the ratio $u = U/J$. At finite temperature in the thermodynamic limit, this transition acquires a classical character, that is, it is governed by thermal fluctuations in a narrow region around a temperature-dependent critical value $u_c(T)$. This thermal transition belongs to the universality class of the three-dimensional (3D) classical XY model. The presence of a harmonic potential $V_{\mathbf{i}}$ implies that different phases may coexist and leads to a modification of the critical value (Fig. 1c). However, this does not prevent the observation of critical scaling[38,39,45]. In our experiment, the total atom number is $N_{\mathrm{tot}} = 4.0(5) \times 10^3$ (Methods), yielding $\langle \hat{n}_{\mathbf{i}} \rangle \approx 1$ at the centre of the system; the control parameter u is tuned between $u \approx 5$ and $u \approx 70$, by adjusting the optical lattice depth.

In classical field theory, the 3D XY transition is associated with a complex-valued order parameter $\psi = |\psi|e^{i\phi}$. In our quantum system, the order parameter is a field operator $\widehat{\psi}$ destroying a particle in the condensate mode[46]. Its squared amplitude $\widehat{N_0} = \widehat{\psi}^{\dagger}\widehat{\psi}$ is an observable that corresponds to the integer-valued number of particles N_0 in the $\mathbf{q} = \mathbf{0}$ quasi-momentum mode. The ordered phase manifests itself through a macroscopic population $N_0 \gg 1$. Our detection method—specific to metastable helium[47]—is ideally suited to reconstruct the full statistics of $|\psi|$ from measuring $|\psi| = \sqrt{N_0}$ in each experimental shot, as it probes the 3D momentum distribution atom by atom (Fig. 2a,b). More details on the apparatus can be found in our previous works[8,48,49] and in the Methods. Figure 2b shows exemplary single-shot experimental realizations. For $u < u_c$, we observe the 3D diffraction pattern associated with a superfluid with long-range phase coherence. Deep in the normal (finite-temperature Mott insulator) regime ($u > u_c$), phase coherence is lost, and the distribution is featureless. For each shot, we denote by N the total detected atom number in the first Brillouin zone (Fig. 2b, blue cube) and $N_0 = |\psi|^2$ is the detected atom number in a sphere of radius $|\delta\mathbf{k}| = 0.03k_d$ centred on $\mathbf{k} = \mathbf{0}$ (Methods). Here, $k_d = 2\pi/d$ is the lattice momentum, where d is the lattice constant. The statistics of N_0 are slightly influenced by the fluctuations of N (Supplementary Information section 1). Post-selecting on N (Fig. 2c) allows us to evaluate and reduce this effect.

We reconstruct the PDF $P(|\psi|)$ from the full counting statistics of N_0 (Methods). The PDFs shown in Fig. 2e exhibit marked differences with u. In the ordered (superfluid) regime, the distribution matches a Gaussian with a maximum around $|\psi_0| \approx 10$, capturing the macroscopic population of the condensate and its expected statistics[35]. In the disordered (Mott) phase, the PDF is different, taking a maximum value for $|\psi_0| = 0$. It is well fitted by a (truncated) Gaussian distribution, as expected from thermal statistics[35,50]. The PDF near the phase transition $u = 37.5$ strongly contrasts with both the ordered and disordered regimes. It features a relatively large width capturing the large fluctuations of the order parameter near u_c and a shape distinct from a Gaussian.

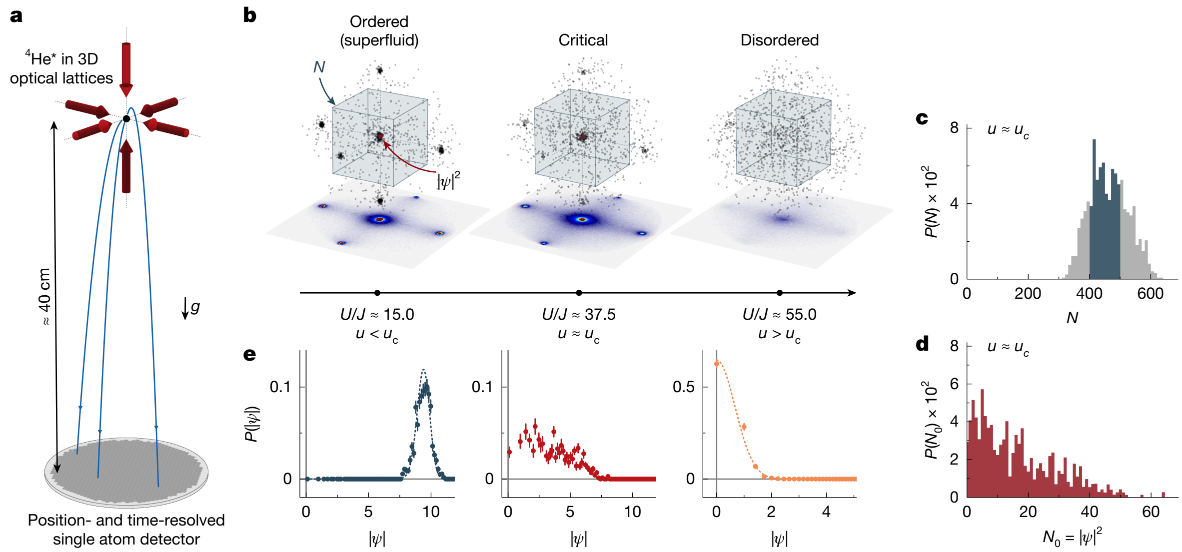

Fig. 2 | Single-atom detection in momentum space and full counting statistics. a, Ultracold ^{4}He* atoms, released from 3D optical lattices, are detected one by one after a free fall onto a micro-channel plate. Their positions and times of arrival allow us to reconstruct their in-trap momenta. **b**, Reconstructed 3D momenta as a function of $u = U/J$. $|\psi|^2$ and N designate, respectively, the number of detected atoms in the central mode ($k/k_d \approx 0$, in red), associated with the condensate and in the first Brillouin zone ($-0.5 \le k_i/k_d \le 0.5$, $i = x, y, z$, blue box). **c**, Probability distribution of the atom number N near the critical point before (grey) and after (blue) post-selection (Methods). Post-selecting on N reduces the effect of shot-to-shot fluctuations on the statistics of N_0 (Supplementary Information section 1). **d**, Probability distribution of the condensate atom number $N_0 = |\psi|^2$ near the critical point, obtained from about 1,200 experimental repetitions. **e**, Probability distributions of the order parameter $|\psi|$. The dashed lines in (i) and (iii) correspond to the expected shapes for the distributions calculated from the measured mean value $\langle|\psi|^2\rangle$ (see text). In this figure and all other figures, error bars represent statistical uncertainties obtained from a bootstrap analysis (Methods).

The shape of the order-parameter PDF is captured by introducing an effective thermodynamic potential $\mathcal{F}(|\psi|) = -\ln P(|\psi|)$. Close enough to the transition, it is well approximated by a low-order polynomial

$$\mathcal{F}(|\psi|) \simeq a_0 + a_2|\psi|^2 + a_4|\psi|^4, \quad (2)$$

similar in spirit to Landau's approach to phase transitions. As detailed in the Supplementary Information, this thermodynamic potential efficiently describes the statistics of the order-parameter amplitude, regardless of the universality class. It has a non-trivial minimum for $a_2 < 0$ (ordered phase) and a minimum at $|\psi| = 0$ for $a_2 > 0$ (disordered phase). Near the transition, $P(|\psi|)$ becomes highly non-Gaussian when $a_2^2/a_4 \lesssim 1$.

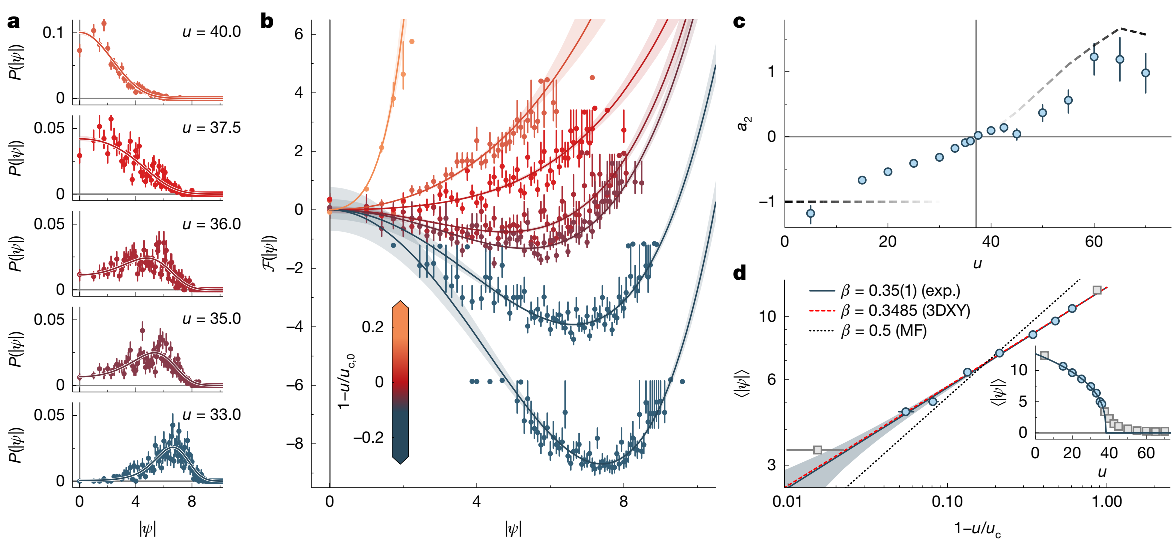

Fig. 3 | Non-Gaussian probability distribution of the order parameter. a, PDF of the order-parameter amplitude $|\psi|$ near the transition in the range $33 \le u \le 40$. The solid lines are fits of the form $P(|\psi|) = e^{-\mathcal{F}(|\psi|)}$, where $\mathcal{F}(|\psi|)$ is given by equation (2). **b**, Effective thermodynamic potential $\mathcal{F}(|\psi|)$ reconstructed from the experimental data shown in **a**, together with $u = 30$ and $u = 55$. **c**, Fitted coefficient a_2 (see equation (2)) as a function of u. The dashed lines correspond to the expected asymptotic behaviours, for $u \ll u_{c,0}$ and $u \gg u_{c,0}$. In the former case, the Poisson statistics of $|\psi|^2$ yield $a_2 = -1$, whereas in the latter case, in which statistics are thermal, we find $a_2 = -\ln[\langle N_0\rangle/(1 + \langle N_0\rangle)]$. The sign change of a_2 marks the critical point $u_{c,0}$ with $u_{c,0} = 37.1(2)$. **d**, Average value $\langle|\psi|\rangle$ as a function of $u_c - u$ for $u < u_c$, showing power-law scaling $\langle|\psi|\rangle \propto (u_c - u)^{\beta}$. The fit yields $u_c = 38.1(2)$ and a critical exponent $\beta = 0.35(1)$ compatible with $\beta_{3DXY} = 0.3485$ (red dashed line), but incompatible with the mean-field prediction $\beta_{MF} = 0.5$ (black dotted line). The inset shows the same quantity as a function of u, with the blue dots representing experimental data points used to extract the coefficient β.

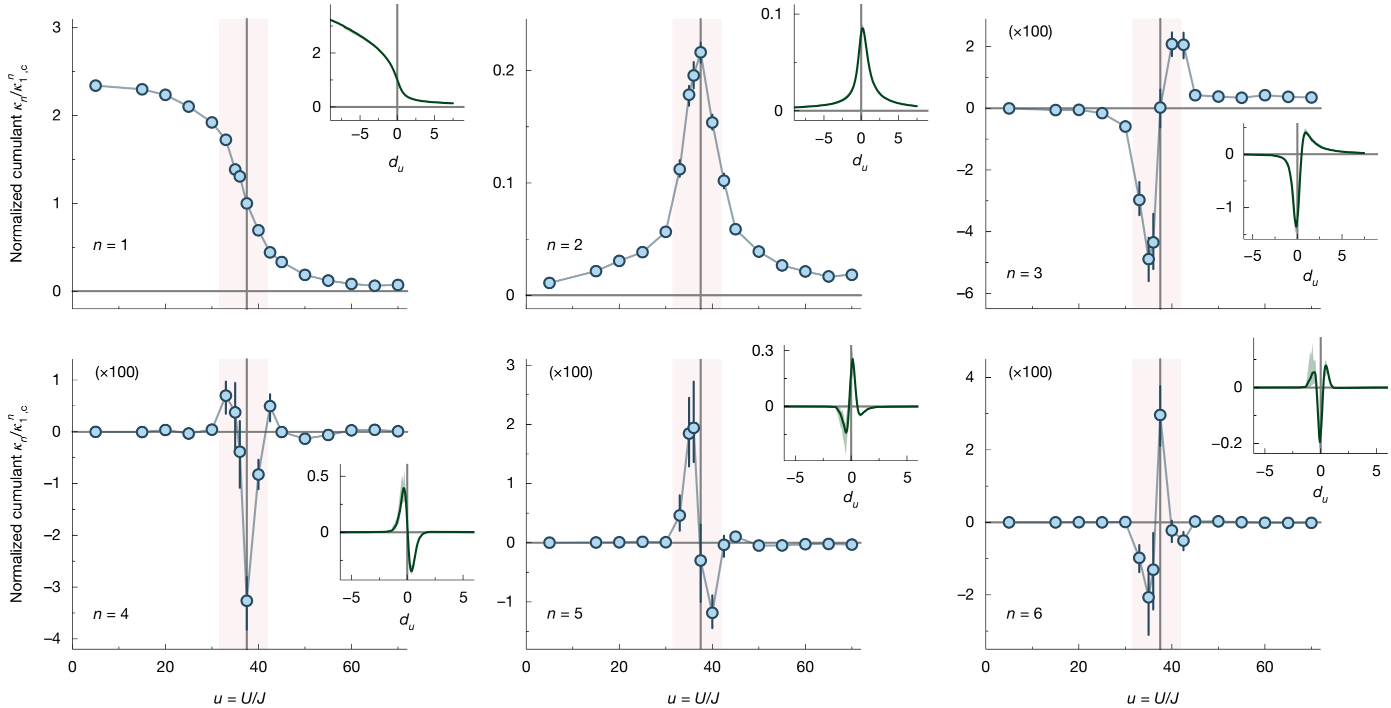

Fig. 4 | Cumulants of the order parameter across the transition. Normalized cumulants $\kappa_n/\kappa^n_{1,c}$ of the order parameter $|\psi|$ up to order $n = 6$ as a function of $u = U/J$, with $\kappa_{1,c} \equiv \kappa_1(u = u_{c,0})$ (Supplementary Information). Significant deviations from zero, observed near the transition point $u = u_{c,0}$ for cumulants of order $n \geq 3$, signal the presence of non-Gaussian fluctuations. The inset shows the universal curve for each cumulant, calculated from a homogeneous quantum rotor model at temperature $T/2Jn_{QR} = 1$, belonging to the 3D XY universality class. The control parameter is rescaled according to $d_u = A(T)(u/u_c - 1)L^{1/\nu}$, where $\nu = 0.6718$ is a critical exponent, L is the linear system size and $A(T)$ is a temperature-dependent coefficient (see text and Supplementary Information).

Figure 3a shows $P(|\psi|)$ measured near the transition, and Fig. 3b shows the corresponding potentials. We observe a continuous change from a distribution similar to that of the ordered phase ($u = 30$), to a distribution closer to the disordered phase ($u = 55$), with flatter distributions in between. Equation (2) fits well our experimental data (Fig. 3a,b, solid lines), with the fitted coefficient a_2 shown in Fig. 3c. As anticipated, a_2 increases from negative to positive values. Empirically, we identify a critical value $u_{c,0} = 37.1(2)$, where a_2 is equal to zero. We stress that, away from the thermodynamic limit, $u_{c,0}$ is different from u_c, the critical point associated with universal scaling. This result is well-established in the phenomenology of finite-size systems[18] (Supplementary Information section 5).

It might seem surprising that our measurements align with the Landau-like mean-field theory, as the probed transition belongs to the 3D XY universality class. However, at fixed u, beyond-mean-field effects manifest themselves only in the tails of the order-parameter PDF, and correspond to rare events[51] (Supplementary Information section 6). Experimentally, the typical number (about 700) of shots used to construct a PDF, although large, remains insufficient to resolve these rare events. By contrast, beyond mean-field effects are revealed by measuring the PDFs on varying the control parameter. This is shown by our measurement of the average value $\langle|\psi|\rangle$ as a function of u (Fig. 3d). First, $\langle|\psi|\rangle$ exhibits power-law scaling with a critical exponent $\beta = 0.35(1)$ compatible with that of the 3D XY universality class, $\beta_{3DXY} = 0.3485$ (ref. 52), and distinct from the mean-field prediction $\beta_{MF} = 0.5$ (Fig. 3d). Second, the critical scaling for $\langle|\psi|\rangle$ is found even for small values of u, suggesting that the critical regime extends deeply into the ordered (superfluid) phase.

The power-law scaling of $\langle|\psi|\rangle$ expected in the thermodynamic limit is observed where the order-parameter PDFs are well captured by Gaussian statistics, that is, where $\xi < L$ as shown in Fig. 1a. Conversely, non-Gaussian statistics appear in a narrower region close to the critical point, at which finite-size effects become important and lead to a breakdown of power-law behaviour. Moreover, the harmonic trap leads to sizeable corrections to u_c, as compared with predictions for a homogeneous system (Fig. 1c). The measured value of $u_c = 38.1(2)$ agrees well with predictions based on Quantum Monte Carlo (QMC) calculations in a harmonic trap[53]. The fact that u_c exceeds the critical value ($u \approx 29.3$) for the superfluid-Mott-insulator quantum phase transition with filling $n = 1$ highlights the fact that the transition occurs in the outer region of the trap, where $n < 1$ (Fig. 5 and Methods).

To quantify explicitly the non-Gaussian nature of the order-parameter statistics close to the critical point, we now focus on its high-order cumulants. Cumulants at all orders reconstruct the full statistical information contained in the PDF, similarly to moments. The cumulant methodology offers a dual advantage. First, cumulants are a standard tool in statistics for capturing non-Gaussian behaviour; the presence of any cumulant $\kappa_{n\geq3} \neq 0$ is necessary and sufficient for non-Gaussian statistics. Second, as we shall see, the dependence of cumulants on the control parameter proves to be extremely rich, providing new and surprising insights into the critical behaviour.

The measured cumulants $\kappa_n(|\psi|)$ of $|\psi|$ are shown in Fig. 4. Cumulants $\kappa_1 = \langle|\psi|\rangle$ and $\kappa_2 = \langle|\psi|^2\rangle - \langle|\psi|\rangle^2$ behave as expected from the phenomenology of a continuous phase transition; κ_1 is finite in the ordered phase ($u \ll u_c$) and vanishes in the disordered phase ($u \gg u_c$), whereas κ_2, which quantifies the order-parameter fluctuations and can be associated with a susceptibility[12], exhibits a peak at $u \approx u_c$.

The evolution of higher-order cumulants with u is instead more instructive. First, cumulants of order $n \geq 3$ vanish deep in the ordered ($u \ll u_c$) and disordered ($u \gg u_c$) phases, whereas they take large values near the phase transition $u \approx u_c$. These variations reveal the crossover of the order-parameter statistics from Gaussian to non-Gaussian across a continuous phase transition. A similar phenomenology has been proposed to identify the phase transition from a hadron gas to a quark-gluon plasma in quantum chromodynamics (QCD)[54–56]. Note that here, the PDF of $|\psi|$ is a truncated Gaussian in the disordered phase, whose cumulants are non-zero and vanish only asymptotically as the

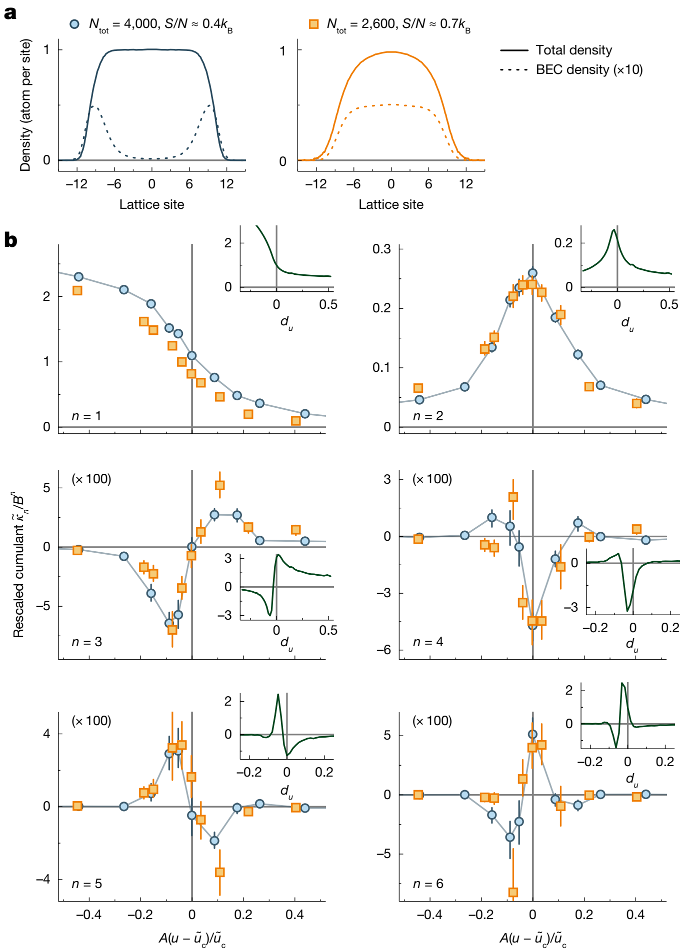

Fig. 5 | Robustness of the cumulant critical behaviour. a, In-trap condensate density (dashed line) and total density (plain line), calculated using QMC under the experimental conditions associated with two experimental data, near their respective critical point $u \approx u_{c,0}$. The volume V of the simulation box is $V = 30^3$ lattice sites. **b**, Measured cumulants expressed in reduced units for the comparison of the two datasets (blue dots correspond to the dataset shown in Fig. 4). The amplitude $\tilde{\kappa}_n = \kappa_n/B^n$ is plotted as a function of a dimensionless distance $A(u - \tilde{u}_c)/\tilde{u}_c$, showing that cumulants coincide at all orders n. A, B and $\tilde{u}_c$ are scale factors determined through a collapse optimization of both datasets (Methods). The insets show cumulants obtained from numerical simulations of the quantum rotor model with $L = 10$ and $T/2Jn_{QR} = 0.05$, that is, in a regime of substantial quantum corrections to the universal scaling (Supplementary Information).

distribution becomes increasingly narrow. Their values are in agreement with the expected thermal statistics[35,50], which are Gaussian. Second, we observe abrupt sign changes of the high-order cumulants near the phase transition. We discuss this unexpected observation below. Before proceeding, we note that the harmonic confinement present in our experiment leads to the coexistence of locally superfluid (or critical) and normal regions. Yet the observed non-Gaussian fluctuations do not stem from the phase coexistence, making the distribution, for example, bimodal (bimodality is not observed). This is because we probe the statistics of a global, rather than local, order parameter, which is always dominated by the superfluid or critical regions in the trap whenever they exist.

In Fig. 4, we first compare the measured cumulants with those obtained numerically in homogeneous models belonging to the 3D XY universality class and find similar sign changes of the cumulants (insets). A finite-size scaling analysis performed on these models—defined on homogeneous lattices with periodic boundary conditions—shows an excellent collapse (Supplementary Fig. 8). This demonstrates that the order-parameter cumulants exhibits universal scaling functions across the phase transition in homogeneous systems.

Although both experiment and simulations show sign changes, we observe qualitative differences for cumulants of order $n \geq 4$. In the critical regime ($L, \xi \gg \ell_G$), universal scaling functions depend not only on the universality class but also on the geometry of the system (boundary conditions, shape of the system and presence of a trap)[57,58]. However, these factors alone cannot account for the differences observed between simulations and experiment in Fig. 4, as we shall now explain. First, numerical simulations of a non-homogeneous classical model yield the same qualitative results as those of homogeneous models (Supplementary Fig. 7). Second, we experimentally tested the effect of the system geometry and found that it does not affect our observations. To this aim, we probed the superfluid transition in a different microscopic configuration (Methods and Extended Data Fig. 1). There, the critical behaviour develops at the trap centre (leading to a substantial shift of u_c), in contrast with the first dataset in which the transition occurs in the outer region of the trap. The results in Fig. 5 show similar behaviour of the cumulants of $|\psi|$ in these two microscopic configurations, confirming that the observed deviations from the classical results are robust to changes in the system geometry. The rescaled units in Fig. 5 make all cumulants $n \geq 2$ coincide, although they are independent of one another.

Instead, we attribute the differences between experiment and 3D XY predictions to universal corrections to scaling induced by quantum fluctuations. Similar corrections are observed in a model of quantum rotors at low temperatures (Fig. 5b (inset) and Supplementary Fig. 9). Only higher-order cumulants are sensitive to these corrections to scaling that affect mostly the tails of the PDF[51]. Our observations highlight that cumulants provide high resolution in the reconstruction of the critical behaviour, exhibiting subtle quantum effects at thermal transitions.

In conclusion, we measured the statistics of the order-parameter amplitude across a continuous phase transition using ultracold lattice bosons. Our experiment is performed in a harmonic trap and realizes an inhomogeneous system of mesoscopic size. We observe many of the emblematic predictions for homogeneous systems, including the change in the effective thermodynamic potential—similar in spirit to Landau theory—and the non-Gaussian critical regime.

Moreover, we experimentally showed abrupt sign changes of the order-parameter cumulants across the transition. We provide numerical evidence and experimental indications of their universal character. These sign changes are general features of criticality, which are not specific to the universality class explored here. They have been observed numerically in the $O(N)$ universality classes[59] and stem from the shape of the critical PDF across the transition[20]. Furthermore, they are considered as promising observables to identify phase transitions in the QCD phase diagram[54–56].

The standard approach of probing critical scaling is achievable in macroscopic systems with negligible finite-size effects. Conversely, our measurement of the order-parameter statistics demonstrates a complementary approach that is well suited to mesoscopic systems. This approach is highly sensitive to the nature of critical fluctuations, including the presence of a quantum phase transition at $T = 0$, and is promising for several quantum-simulation platforms[25–28,30,31]. Furthermore, the experimental ability to reconstruct the order-parameter fluctuations in finite-size inhomogeneous systems challenges theoretical and numerical methods for quantum systems.

Online content

Any methods, additional references, Nature Portfolio reporting summaries, source data, extended data, supplementary information, acknowledgements, peer review information; details of author contributions and competing interests; and statements of data and code availability are available at https://doi.org/10.1038/s41586-026-10811-1.

1. Zinn-Justin, J. *Quantum Field Theory and Critical Phenomena* Vol. 113 of International Series of Monographs on Physics (Oxford Univ. Press, 2002).
2. Binder, K. Critical properties from Monte Carlo coarse graining and renormalization. *Phys. Rev. Lett.* **47**, 693–696 (1981).
3. Bruce, A. D. & Wilding, N. B. Scaling fields and universality of the liquid-gas critical point. *Phys. Rev. Lett.* **68**, 193–196 (1992).
4. Bouchaud, J.-P. & Georges, A. Anomalous diffusion in disordered media: statistical mechanisms, models and physical applications. *Phys. Rep.* **195**, 127–293 (1990).
5. Bramwell, S. T., Holdsworth, P. C. W. & Pinton, J.-F. Universality of rare fluctuations in turbulence and critical phenomena. *Nature* **396**, 552–554 (1998).
6. Botet, R. & Ploszajczak, M. *Universal Fluctuations. The Phenomenology of Hadronic Matter*. No. 65 in Lecture Notes in Physics Series (World Scientific, 2002).
7. Joubaud, S., Petrosyan, A., Ciliberto, S. & Garnier, N. B. Experimental evidence of non-Gaussian fluctuations near a critical point. *Phys. Rev. Lett.* **100**, 180601 (2008).
8. Cayla, H. et al. Single-atom-resolved probing of lattice gases in momentum space. *Phys. Rev. A* **97**, 061609 (2018).
9. Greiner, M., Mandel, O., Esslinger, T., Hänsch, T. W. & Bloch, I. Quantum phase transition from a superfluid to a Mott insulator in a gas of ultracold atoms. *Nature* **415**, 39–44 (2002).
10. Landau, L. D. On the theory of phase transitions. *Zh. Eksp. Teor. Fiz.* **7**, 19–32 (1937).
11. Ginzburg, V. L. & Landau, L. D. On the theory of superconductivity. *Zh. Eksp. Teor. Fiz.* **20**, 1064–1082 (1950).
12. Nishimori, H. & Ortiz, G. *Elements of Phase Transitions and Critical Phenomena* (Oxford Univ. Press, 2010).
13. Bramwell, S. T. et al. Magnetic fluctuations in the classical XY model: the origin of an exponential tail in a complex system. *Phys. Rev. E* **63**, 041106 (2001).
14. Wilson, K. G. & Kogut, J. The renormalization group and the ϵ expansion. *Phys. Rep.* **12**, 75–199 (1974).
15. Fisher, M. E. Renormalization group theory: its basis and formulation in statistical physics. *Rev. Mod. Phys.* **70**, 653–681 (1998).
16. Chen, X. S., Dohm, V. & Schultka, N. Order-parameter distribution function of finite $O(n)$ symmetric systems. *Phys. Rev. Lett.* **77**, 3641–3644 (1996).
17. Tsypin, M. M. & Blöte, H. W. J. Probability distribution of the order parameter for the three-dimensional Ising-model universality class: a high-precision Monte Carlo study. *Phys. Rev. E* **62**, 73–76 (2000).
18. Balog, I., Rançon, A. & Delamotte, B. Critical probability distributions of the order parameter from the functional renormalization group. *Phys. Rev. Lett.* **129**, 210602 (2022).
19. Sahu, S., Delamotte, B. & Rançon, A. Generalization of the central limit theorem to critical systems: revisiting perturbation theory. *Phys. Rev. E* **111**, 034128 (2025).
20. Rançon, A., Delamotte, B., Šaravanja, L. & Balog, I. Probability distributions of the order parameter of the $O(N)$ model. *Phys. Rev. E* **111**, 034131 (2025).
21. Hsu, S.-Y., Chervenak, J. A. & Valles, J. M. Jr Magnetic field enhanced order parameter amplitude fluctuations in ultrathin Films near the superconductor-insulator transition. *Phys. Rev. Lett.* **75**, 132–135 (1995).
22. Takeuchi, K. A. & Sano, M. Universal fluctuations of growing interfaces: evidence in turbulent liquid crystals. *Phys. Rev. Lett.* **104**, 230601 (2010).
23. Sornette, D. *Critical Phenomena in Natural Sciences: Chaos, Fractals, Selforganization and Disorder: Concepts and Tools* (Springer, 2006).
24. Islam, R. et al. Onset of a quantum phase transition with a trapped ion quantum simulator. *Nat. Commun.* **2**, 377 (2011).
25. Jurcevic, P. et al. Direct observation of dynamical quantum phase transitions in an interacting many-body system. *Phys. Rev. Lett.* **119**, 080501 (2017).
26. Makhalov, V. et al. Probing quantum criticality and symmetry breaking at the microscopic level. *Phys. Rev. Lett.* **123**, 120601 (2019).
27. Xu, K. et al. Probing dynamical phase transitions with a superconducting quantum simulator. *Sci. Adv.* **6**, eaba4935 (2020).
28. Ebadi, S. et al. Quantum phases of matter on a 256-atom programmable quantum simulator. *Nature* **595**, 227–232 (2021).
29. Fontaine, Q. et al. Kardar-Parisi-Zhang universality in a one-dimensional polariton condensate. *Nature* **608**, 687–691 (2022).
30. Chen, C. et al. Continuous symmetry breaking in a two-dimensional Rydberg array. *Nature* **616**, 691–695 (2023).
31. Ho, J. et al. Optomechanical self-organization in a mesoscopic atom array. *Nat. Phys.* **21**, 1071–1077 (2025).
32. Ott, H. Single atom detection in ultracold quantum gases: a review of current progress. *Rep. Prog. Phys.* **79**, 054401 (2016).
33. Bohnet, J. G. et al. Quantum spin dynamics and entanglement generation with hundreds of trapped ions. *Science* **352**, 1297–1301 (2016).
34. Schweigler, T. et al. Experimental characterization of a quantum many-body system via higher-order correlations. *Nature* **545**, 323–326 (2017).
35. Hercé, G. et al. Full counting statistics of interacting lattice gases after an expansion: the role of condensate depletion in many-body coherence. *Phys. Rev. Res.* **5**, L012037 (2023).
36. Joshi, L. K., Ares, F., Joshi, M. K., Roos, C. F. & Calabrese, P. Measuring full counting statistics in a trapped-ion quantum simulator. *Phys. Rev. Lett.* **135**, 160601 (2025).
37. Pelissetto, A. & Vicari, E. Critical phenomena and renormalization-group theory. *Phys. Rep.* **368**, 549–727 (2002).
38. Donner, T. et al. Critical behavior of a trapped interacting Bose gas. *Science* **315**, 1556–1558 (2007).
39. Zhang, X., Hung, C.-L., Tung, S.-K. & Chin, C. Observation of quantum criticality with ultracold atoms in optical lattices. *Science* **335**, 1070–1072 (2012).
40. Shao, H.-J. et al. Antiferromagnetic phase transition in a 3D fermionic Hubbard model. *Nature* **632**, 267–272 (2024).
41. Bertin, E. Global fluctuations and Gumbel statistics. *Phys. Rev. Lett.* **95**, 170601 (2005).
42. Coleman, P. & Schofield, A. J. Quantum criticality. *Nature* **433**, 226–229 (2005).
43. Carcy, C., Hercé, G., Tenart, A., Roscilde, T. & Clément, D. Certifying the adiabatic preparation of ultracold lattice bosons in the vicinity of the Mott transition. *Phys. Rev. Lett.* **126**, 045301 (2021).
44. Fisher, M. P. A., Weichman, P. B., Grinstein, G. & Fisher, D. S. Boson localization and the superfluid-insulator transition. *Phys. Rev. B* **40**, 546–570 (1989).
45. Campostrini, M. & Vicari, E. Critical behavior and scaling in trapped systems. *Phys. Rev. Lett.* **102**, 240601 (2009).
46. Pitaevskii, L. & Stringari, S. *Bose-Einstein Condensation and Superfluidity* Vol. 164 (Oxford Univ. Press, 2016).
47. Vassen, W. et al. Cold and trapped metastable noble gases. *Rev. Mod. Phys.* **84**, 175–210 (2012).
48. Tenart, A., Hercé, G., Bureik, J.-P., Dareau, A. & Clément, D. Observation of pairs of atoms at opposite momenta in an equilibrium interacting Bose gas. *Nat. Phys.* **17**, 1364–1368 (2021).
49. Bureik, J.-P. et al. Suppression of Bogoliubov momentum pairing and emergence of non-Gaussian correlations in ultracold interacting Bose gases. *Nat. Phys.* **21**, 57–62 (2025).
50. Carcy, C. et al. Momentum-space atom correlations in a Mott insulator. *Phys. Rev. X* **9**, 041028 (2019).
51. Balog, I., Delamotte, B. & Rançon, A. Universal and non-universal large deviations in critical systems. *SciPost Phys.* **18**, 119 (2025).
52. Campostrini, M., Hasenbusch, M., Pelissetto, A., Rossi, P. & Vicari, E. Critical behavior of the three-dimensional XY universality class. *Phys. Rev. B* **63**, 214503 (2001).
53. Hercé, G. et al. Studying the low-entropy Mott transition of bosons in a three-dimensional optical lattice by measuring the full momentum-space density. *Phys. Rev. A* **104**, L011301 (2021).
54. Stephanov, M. A. Sign of kurtosis near the QCD critical point. *Phys. Rev. Lett.* **107**, 052301 (2011).
55. Asakawa, M., Ejiri, S. & Kitazawa, M. Third moments of conserved charges as probes of QCD phase structure. *Phys. Rev. Lett.* **103**, 262301 (2009).
56. Bzdak, A. et al. Mapping the phases of quantum chromodynamics with beam energy scan. *Phys. Rep.* **853**, 1–87 (2020).
57. Vasilyev, O., Gambassi, A., Maciołek, A. & Dietrich, S. Universal scaling functions of critical Casimir forces obtained by Monte Carlo simulations. *Phys. Rev. E* **79**, 041142 (2009).
58. Hucht, A., Grüneberg, D. & Schmidt, F. M. Aspect-ratio dependence of thermodynamic Casimir forces. *Phys. Rev. E* **83**, 051101 (2011).
59. Pan, X., Chen, L., Chen, X. S. & Wu, Y. High-order cumulants from the 3-dimensional $O(1, 2, 4)$ spin models. *Nucl. Phys. A* **913**, 206–216 (2013).

Methods

Production of low-entropy and low-number Bose–Einstein condensates

Our experiment uses standard laser cooling and evaporative cooling steps to produce a spin-polarized Bose–Einstein condensate (BEC) of about 4×10^5 metastable helium-4 (^{4}He*) in the sub-level $m_J = 1$ of the state 2^3S_1 (ref. 60). The atom number is then reduced to $4.0(5) \times 10^3$ ($2.6(3) \times 10^3$ for the second dataset) using state-dependent inelastic losses. We use two-photon Raman transitions to transfer a controlled fraction of the atoms to the sub-level $m_J = 0$, where two-body Penning ionization leads to losses. The small BEC is then loaded adiabatically in the cubic optical lattice. In the 3D lattice, the trapping frequency of the harmonic potential V_t is $\omega/2\pi = 140(5)\sqrt{V_0}$ Hz, where V_0 is the lattice amplitude in units of the recoil energy $E_\mathrm{R} = h^2/8md^2$, and m is the mass of an atom. A thermometry based on the comparison with ab initio QMC calculations[43] yields a temperature in the range of $k_\mathrm{B}T/J \sim$ 1.5–2. This is compatible with an entropy per atom of $S/N \sim 0.4(1)k_\mathrm{B}$ ($0.7(1)k_\mathrm{B}$ for the second dataset) extracted from the measured condensate fraction before loading the BEC in the optical lattices[43].

Volume used to compute the statistics of $|\psi|$

In translationally invariant lattice systems, where the quasi-momentum $\mathbf{q}$ is a good quantum number, the number of condensate atoms N_0 is equal to the atom number in the mode $\mathbf{q} = \mathbf{0}$. In a finite-size and harmonically trapped gas, N_0 remains well approximated by the atom number at $\mathbf{q} = \mathbf{0}$. In this work, we probe the gas in the momentum basis, where the modes located at $\mathbf{n}k_\mathrm{d}$, with $\boldsymbol{n} \in \mathbb{Z}^3$, are copies of the mode $\mathbf{q} = \mathbf{0}$. We use a sphere of radius $0.03k_\mathrm{d}$ centred on the central peak ($\mathbf{n} = \mathbf{0}$) or first-order diffraction peaks ($\|\boldsymbol{n}\| = 1$) to measure N_0 in each shot. This radius is unambiguously determined from the width of the bosonic bunching signal, which is set by the size of one mode[50,61]. As shown in the Supplementary Information, the exact value of the radius we use in the analysis does not affect our observations.

PDF and cumulants of $|\psi|$

The PDF of $|\psi| = \sqrt{N_0}$ is reconstructed from the histogram of the measured values of the condensate atom number N_0 in each shot. The histogram bins for the discrete variable N_0 are the positive integers, and the histogram is normalized such that it sums to one, $\sum_n P(N_0 = n) = 1$. The PDF of $|\psi|$ is obtained by remarking that $P(N_0 = n) = P(|\psi| = \sqrt{n})$. Its normalization is set by that of the histogram on N_0.

The cumulants of $|\psi|$ in Figs. 4 and 5b are computed directly from the measured values of $\sqrt{N_0}$. They are normalized by $\langle\sqrt{N}\rangle^n$ to account for the variation of the atom number N in the first Brillouin zone with the interaction parameter u.

Bootstrap procedure

The error bars on experimental cumulants, PDFs and fit parameters are 68% confidence intervals obtained from a bootstrap method. Five hundred pseudosamples are generated from sampling the experimental shots with replacement. The observables are computed for each pseudosample. The resulting histograms take a typical bell-shape curve, from which the mean, the 16th and 84th percentiles are extracted. The percentiles provide an estimate of the statistical uncertainty on the mean.

Trapped atomic densities at different total atom number

In Fig. 5, we compare the order-parameter cumulants measured in lattice gases with different total atom numbers and entropy per atom. As discussed in the main text and shown in Extended Data Fig. 1, the difference in the measured critical values $u_{\mathrm{c},0}$ highlights the distinct configurations of in-trap densities close to $u_{\mathrm{c},0}$: at small atom number, the condensate develops at the trap centre. By contrast, the condensate appears in the outer region of the trap at a large atomic number. These differences are confirmed by numerical calculations of the harmonically trapped Bose–Hubbard Hamiltonian using QMC[43] (Fig. 5a). There we contrast the local density $n_i = \langle\hat{a}_i^\dagger\hat{a}_i\rangle$ with the condensate density $n_i^{(0)} = \frac{1}{V}\sum_j \langle\hat{a}_i^\dagger\hat{a}_j\rangle$, where V is the volume of the simulation box. All the parameters used in these numerical calculations are calibrated from the experiment, except for the temperature, which is estimated by matching the momentum distribution calculated numerically by QMC with that measured experimentally, as described in ref. 43.

Cumulants in rescaled units

The cumulants measured for different microscopic configurations of the trapped gas are shown in Fig. 5 in rescaled units inspired by theoretical approaches to critical collapse. The ratio $u = U/J$ is replaced by the distance $A\delta u$ to the critical point, with $\delta u = (u - \tilde{u}_\mathrm{c})/\tilde{u}_\mathrm{c}$, and the amplitudes of the cumulants κ_n are rescaled as $\tilde{\kappa}_n = \kappa_n/B^n$. The parameters A, B and $\tilde{u}_\mathrm{c}$ are specific to a microscopic configuration, whereas the function $\tilde{\kappa}_n(A\delta u)$ is expected to be independent of the configuration when it describes universal behaviour.

In our procedure, the non-universal scaling factors are obtained by minimizing the cumulative error (the sum of squared differences computed over the second through sixth cumulants) between the two datasets after rescaling. We arbitrarily chose the second dataset (Fig. 5, orange squares) as a reference—setting $A = 1$ and $B = 1$ and the value $\tilde{u}_\mathrm{c} = u_{\mathrm{c},0}$ determined from $a_2 = 0$—and numerically optimize the scaling factors A, B and $\tilde{u}_\mathrm{c}$ of the first dataset (Figs. 4 and 5, blue circles). Because the data points are discrete and not aligned after rescaling, the values of $\tilde{\kappa}_n$ for one dataset are interpolated linearly to compute the error with respect to the other dataset. The fitted values for the first dataset are $A = 1.32(8)$, $B = 0.91(1)$ and $\tilde{u}_\mathrm{c} = 37.5(1)$, that is, the fitted value for $\tilde{u}_\mathrm{c}$ is close to $u_{\mathrm{c},0} = 37.1(2)$, determined from $a_2 = 0$ (see the main text).

Data availability

The datasets generated and analysed in the present study, as well as the code used for the analysis, are available from the corresponding author upon request. Source data are provided with this paper.

Code availability

The numerical code used to generate the plot in this work is available from the corresponding author upon request.

60. Bouton, Q. et al. Fast production of Bose-Einstein condensates of metastable helium. *Phys. Rev. A* **91**, 061402 (2015).
61. Cayla, H. et al. Hanbury Brown and Twiss bunching of phonons and of the quantum depletion in an interacting Bose gas. *Phys. Rev. Lett.* **125**, 165301 (2020).

Acknowledgements We thank I. Balog, A. Browaeys, Z. Hadzibabic and the members of the Quantum Gas group at the Institut d'Optique for their discussions. Numerical simulations were conducted on the CPBsmn cluster at the ENS of Lyon.

Author contributions M.A., G.D. and P.P. carried out the experiments. A.R. and T.R. conducted the numerical simulations. M.A., G.D., P.P., N.D., A.R., T.R., T.C. and D.C. contributed to the data analysis, progression of the project and writing of the paper.

Funding We acknowledge funding from the Région Ile-de-France in the framework of the DIM QuanTiP, the 'Fondation d'entreprise iXcore pour la Recherche', the French National Research Agency (grant no. ANR-17-CE30-0020-01) and France 2030 programs of the French National Research Agency (grant no. ANR-22-PETQ-0004). A.R. has benefited from the financial support of the grant no. ANR-24-CE30-6695 FUSIoN.

Competing interests The authors declare no competing interests.

Additional information
Supplementary information The online version contains supplementary material available at https://doi.org/10.1038/s41586-026-10811-1.
Correspondence and requests for materials should be addressed to David Clément.
Peer review information *Nature* thanks the anonymous reviewers for their contribution to the peer review of this work. Peer reviewer reports are available.
Reprints and permissions information is available at http://www.nature.com/reprints.

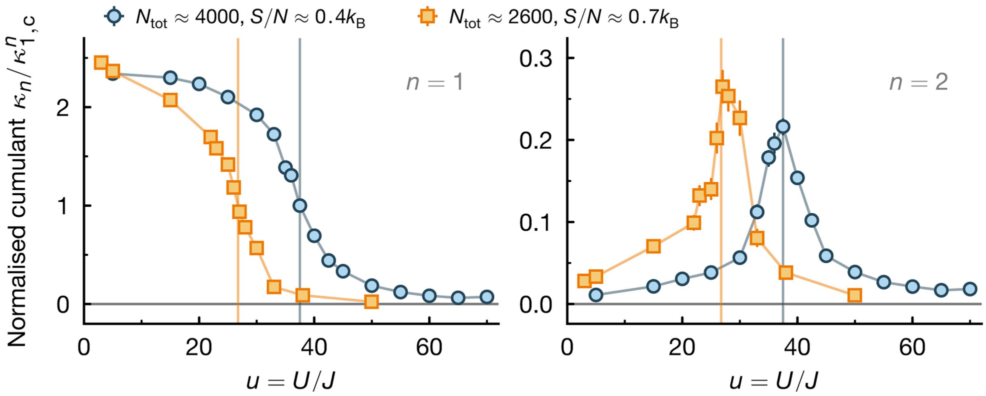

Extended Data Fig. 1 | Mean and variance of the order parameter in two distinct microscopic configurations. Normalised mean $\kappa_1/\kappa_{1,c}$ and variance $\kappa_2/\kappa_{1,c}^2$ of the order-parameter amplitude measured in the two datasets analysed in Fig. 5. The vertical lines depict the critical values $u_{c,0}$ of the respective datasets.